Universiteit
Leiden
The Netherlands

Blood flow dynamics in the total cavopulmonary connection long-term after Fontan completion

Rijnberg, F.M.

Citation
Rijnberg, F. M. (2023, December 20). *Blood flow dynamics in the total cavopulmonary connection long-term after Fontan completion*. Retrieved from https://hdl.handle.net/1887/3674148

Version:	Publisher's Version
License:	Licence agreement concerning inclusion of doctoral thesis in the Institutional Repository of the University of Leiden
Downloaded from:	https://hdl.handle.net/1887/3674148

Note: To cite this publication please use the final published version (if applicable).

CHAPTER 10

10

Non-uniform mixing of hepatic venous flow and inferior vena cava flow in the Fontan conduit

Rijnberg FM, van der Woude SFS, van Assen HC, Juffermans JF, Hazekamp MG, Jongbloed MRM, Kenjeres S, Lamb HJ, Westenberg JJM, Wentzel JJ, Roest AAW

Journal of the Royal Society Interface 2021

Abstract

Background

Fontan patients require a balanced hepatic blood flow distribution (HFD) to prevent pulmonary arteriovenous malformations. Currently, HFD is quantified by tracking Fontan conduit flow, assuming hepatic venous (HV) flow to be uniformly distributed within the Fontan conduit. However, this assumption may be unvalid leading to inaccuracies in HFD quantification with potential clinical impact. The aim of this study was to 1) assess mixing of HV flow and inferior vena caval (IVC) flow within the Fontan conduit and 2) quantify HFD by directly tracking HV flow and quantitatively compare results with the conventional approach.

Methods

Patient-specific, time-resolved computational fluid dynamic models of 15 total cavopulmonary connections (TCPC) were generated, including the hepatic veins (HV) and subhepatic IVC. Mixing of HV and IVC flow, on a scale between 0 (no mixing) and 1 (perfect mixing), was assessed at the caudal and cranial Fontan conduit. HFD was quantified by tracking particles from the caudal ($HFD_{caudal\ conduit}$) and cranial ($HFD_{cranial\ conduit}$) conduit and from the hepatic veins (HFD_{HV}).

Results

HV flow was non-uniformly distributed at both the caudal (mean mixing 0.66±0.13) and cranial (mean 0.79±0.11) level within the Fontan conduit. On a cohort-level, differences in HFD between methods were significant but small; HFD_{HV} (51.0±20.6%) versus $HFD_{caudal\ conduit}$ (48.2±21.9%, p=0.033) or $HFD_{cranial\ conduit}$ (48.0±21.9%, p=0.044). However, individual absolute differences of 8.2-14.9% in HFD were observed in 4/15 patients.

Conclusion

HV flow is non-uniformly distributed within the Fontan conduit. Substantial individual inaccuracies in HFD quantification were observed in a subset of patients with potential clinical impact.

Introduction

The Fontan operation is the palliative procedure for single ventricle patients, in which both venae cavae are connected with the pulmonary arteries (PAs), also called the total cavopulmonary connection (TCPC). The TCPC needs to ensure a balanced hepatic venous flow distribution (HFD), containing an important hepatic factor, towards both lungs[1]. A lack of hepatic factor has been associated with the formation of pulmonary arteriovenous malformations in the affected lung, leading to progressive hypoxemia, cyanosis and exercise intolerance[2].

In recent years, patient-specific platforms using a combination of computational fluid dynamics (CFD) and magnetic resonance imaging (MRI) are emerging as a valuable tool for clinicians for evaluating HFD and power loss[3, 4]. In addition, these platforms allow for performing "virtual surgery", by which multiple different TCPC geometries can be virtually created and associated blood flow can be predicted. Subsequently, the optimal TCPC geometry with minimal power loss and a balanced HFD can be determined guiding surgical and catheter-based interventions[5, 6].

HFD can be determined with particle tracing techniques using 4D flow MRI[7-11] or computational fluid dynamic models (CFD)[12]. Conventional HFD quantification methods track particles that are uniformly seeded within the Fontan conduit and determine the distribution of these particles towards both PAs. Therefore, this method relies on the unvalidated assumption that hepatic blood is uniformly distributed within the Fontan conduit[13, 14]. However, since blood flow is laminar in the inferior vena cava (IVC) and Fontan conduit, the mixing of hepatic blood with IVC blood might be less optimal than generally assumed. We hypothesized that there is a non-uniform distribution of hepatic venous flow in the Fontan conduit that affects the accuracy of the current HFD quantification approach. These inaccuracies have potential consequences for identification of patients with unbalanced HFD, or by affecting optimal TCPC model selection in virtual surgery platforms. The aim of this study was twofold: 1) to test the hypothesis of non-uniform hepatic blood distribution within the Fontan conduit by quantification of mixing between IVC and hepatic venous flow within the Fontan conduit, and 2) to quantify HFD from the level of the Fontan conduit (conventional method), as well as from the level of the hepatic veins (HVs, direct method).

Methods

Patient population

Fifteen Fontan patients were included that underwent MRI as part of a prospective study between November 2018-May 2019 at the Leiden University Medical Center. All patients >8 years old without contraindications for MRI were eligible for inclusion. Patient characteristics are provided in Table 1. The study was approved by the institutional review board of the hospital. Informed consent was obtained from all subjects and/or their guardians.

Magnetic resonance imaging

MRI acquisitions details are provided in Supplementary Table 1. Transversal and sagittal stacks of static, respiratory-compensated 2D anatomic images were acquired for segmentation of the TCPC. Free-breathing, two-dimensional phase-contrast MRI (2D PC-MRI) with three-directional velocity encoding was acquired at the following locations: subhepatic IVC, Fontan conduit, superior vena cava (SVC), right (RPA) and left PAs (LPA). In this study, flow was quantified using the (clinically standard) through-plane velocity direction only (CAAS MR Solutions v5.1, Pie Medical Imaging, Maastricht, the Netherlands). Total hepatic venous flow was determined by subtracting IVC flow from Fontan conduit flow.

3D TCPC model creation

A detailed description of the TCPC segmentation and CFD analysis are provided in Supplementary Material 1. The TCPC was segmented using both sagittal and transversal stacks, covering the area between the subhepatic IVC, hepatic veins, SVC, RPA and LPA (ITK-SNAP[15]). Segmental branches were excluded, except for the right upper lobe branches. A 3D TCPC model was created, smoothed and centerlines were derived for each vessel (VMTK[16]).

CFD simulations

All inlets and outlets of the 3D TCPC model were clipped perpendicular to the centerlines. Furthermore, vessel extensions were added to the entrances and exits of the model. Using these vessel extensions, the inflow velocity profiles at the entrances of the 3D TCPC model were fully developed and resembled the velocity profiles at those locations. After adding vessel extensions at all in- and outlets, the 3D TCPC models were meshed with 30 polyhedral elements across the average vessel diameter (range 0.4-0.5mm elements) in order to achieve mesh-independent results (ANSYS ICEM v17.1, Inc., Canonsburg, PA)[17]. All CFD simulations were performed using commercially available Fluent software (v17.1, ANSYS, Inc., Canonsburg, PA).

Time-resolved flowrates were prescribed with a parabolic velocity profile at the inlets. Total hepatic venous flow was divided over the multiple hepatic veins based on the ratio of their respective cross-sectional areas. Outlet boundary conditions were imposed based on the ratio of measured pulmonary flow distribution (RPA/LPA flow divided by the total PA flow)[3]. A rigid vessel wall was assumed and a no-slip condition prescribed. Blood flow was assumed to be laminar. A Carreau model was used to account for the non-Newtonian blood properties in the TCPC[18].

Quantification of mixing between IVC and Hepatic blood flow

A method to quantify mixing of hepatic and IVC blood flow within the Fontan conduit was developed based on the spatial distribution of both flows within the Fontan conduit using particle tracing (Paraview.org). A total of 7500 particles were released from the hepatic veins for each time-step during 5 cardiac cycles. The number of particles per hepatic vein was based on the ratio of their respective cross-sectional areas. The amount of particles released from the subhepatic IVC was based on the average flow ratio between the IVC and hepatic veins; 7500 x $\frac{Q_{IVC}}{Q_{HV}}$.

Particles were released from the HVs and IVC for each time-step during 5 cardiac cycles.

Pathlines, representing the trajectory each particle follows over time, were generated and transections with these pathlines were made at two cross-sections with the Fontan conduit: the caudal part of the Fontan conduit, just above the connection between the Fontan conduit with the IVC/HVs, and at the cranial part of the Fontan conduit, just below the connection with the PA (Figure 1A-C, Video 1). The ratio of IVC and HV pathline transections at each cross-section of the Fontan conduit were recorded for each time-step in the 5th cardiac cycle.

Subsequently, both caudal and cranial Fontan conduit cross-sections were manually subdivided in a right-left and anterior-posterior direction, resulting in four subsections: left-anterior, left-posterior, right-anterior and right-posterior (Figure 1B-C). The ratio of IVC and HV pathline transections was determined in each of the four subsections. Next, mixing (M) in each of the four subsections was determined for each time-phase of the cardiac cycle by comparing the ratios of IVC and HV pathline transections within the entire cross-section with the ratios of IVC and HV pathline transsections within each of the four subsections, ranging from 0 (no mixing) to 1 (perfect mixing). A mixing of 0 indicates no mixing (only HV or IVC pathlines present in the subsection) and 1 indicates perfect mixing (the exact same ratio of HV and IVC pathlines in the subsection as in the entire cross-section). Furthermore, cardiac-cycle averaged mixing ($M_{average}$) was determined for each subsection and for the entire cross-section. A detailed description of the mixing quantification method is provided in Supplementary material 2.

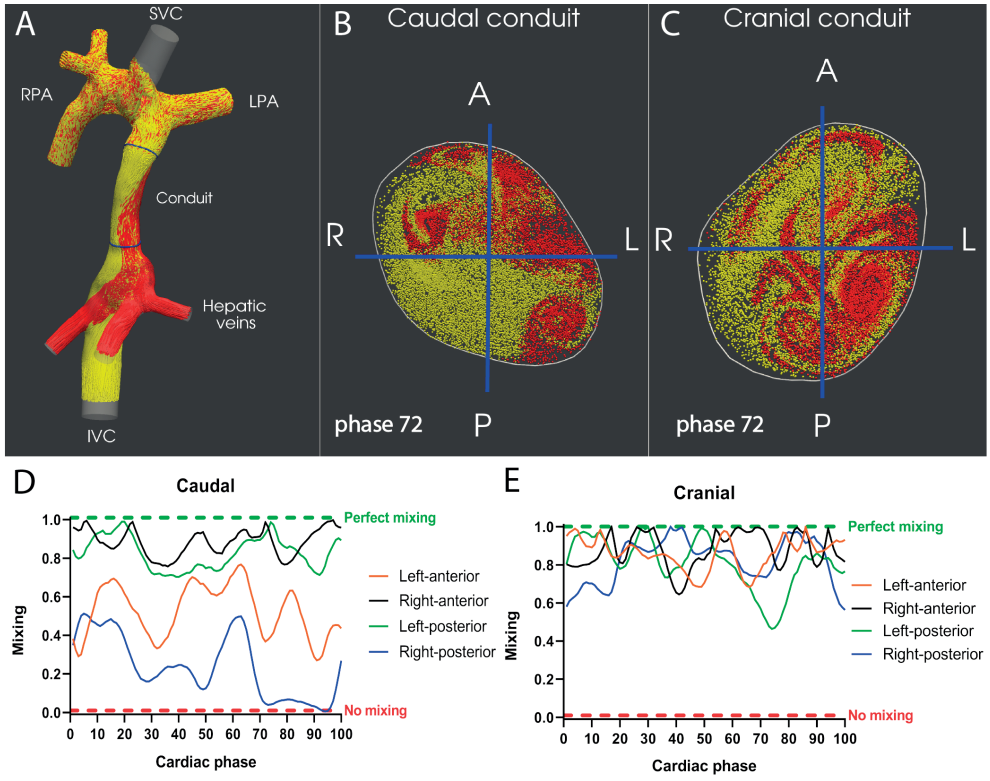

Figure 1. (A) Pathlines originating from the hepatic veins (HV, red) and inferior vena cava (IVC, yellow) are shown within the TCPC of a typical extracardiac conduit Fontan patient. Positions of the caudal and cranial cross-sections with the Fontan conduit are shown (blue). Of note, no pathlines were generated from the superior vena cava to allow for better visualization of the HV and IVC flow. **(B-C)** Transections with HV and IVC pathlines are shown for the caudal **(B)** and cranial **(C)** cross-sections for phase 72/100 of the cardiac cycle. The division into four subsections is indicated by blue lines. Note how a evidently non-uniform distribution of HV flow is present, most strikingly at the caudal part of the conduit, with almost no HV flow present in the right-posterior subsection. **(D-E)** Time-resolved mixing characteristics of HV and IVC flows are shown for the caudal and cranial cross-section of the conduit. At the caudal conduit, a relatively good mixing is present in the right-anterior and left-posterior subsections, with reduced mixing in the left-anterior and right-posterior segments. Note how almost no mixing is present at phase 72 in the right-posterior segment, consistent with the absence of HV flow in this subsection **(B)**. **(E)** Significantly better mixing is present at the cranial part of the conduit, illustrated by a more uniform distribution of IVC and HV flow streams over the cross-section.

SVC/IVC; superior/inferior vena cava, LPA/RPA; left/right pulmonary artery, A; anterior, P; posterior, L/R; left/right

HFD quantification

HFD was quantified using particle tracing[7, 13, 19], by seeding 7500 particles from either the HVs ($HFD_{HV:}$ direct method) or from the level of one of the 2 cross-sections ($HFD_{caudal\ conduit}$ and $HFD_{cranial\ conduit:}$ conventional method, Figure 2). The 7500 particles were divided over the hepatic veins based on the ratio of their respective areas. Particles were released

for 100 time-steps (1 cardiac cycle) and particles arriving at the PAs were recorded for 500-1200 timesteps (5-12 cardiac cycles) to allow for sufficient transit time for particles to reach the PAs. HFD is defined as the ratio of particles exiting through the LPA with respect to the total number of particles reaching either PA[13]:

HFD = $\frac{P_{LPA}}{P_{RPA}+P_{LPA}} * 100\%$, where P is the number of particles arriving in each PA, respectively.

Statistical analysis

Mixing (M) of HV flow in the Fontan conduit was defined as follows: no mixing <0.1, poor mixing 0.1-0.3, mild mixing 0.3-0.5, moderate mixing 0.5-0.7, good mixing 0.7-0.9, uniform mixing >0.9. Bland-Altman plots and intraclass correlation (ICC) analysis were used to assess agreement between HFD methods. The mean absolute difference (± 1.96 standard error of the mean) between methods was quantified to determine the absolute amount of which one HFD quantification method over- or underestimates the other method. All differences were reported in percentage points. Measurements were compared using a paired t-test. $M_{average}$ between subsections was compared using a repeated measurements one-way ANOVA test with post-hoc analysis (Tukey). A p-value <0.05 was considered statistically significant. Continuous data were presented as mean±SD. Data were analyzed with SPSS 25.0 and Prism 8.0.

Results

Patient characteristics and MRI flow measurements are presented in Table 1.

Mixing of IVC and HV flow

An evident streaming pattern of HV flow within the Fontan conduit was present resulting in non-uniform distribution of HV flow within the Fontan conduit, most evidently shown in the caudal part of the Fontan conduit (Figure 1A-B, Supplemental Video 1). This observation was also reflected by a significant lower cardiac-cycle averaged mixing ($M_{average}$) in the caudal (moderate mixing, mean 0.66±0.13) compared to the cranial part of the Fontan conduit (good mixing, mean 0.79±0.11, p<0.001). $M_{average}$ over the entire cross-section at both the caudal and cranial level of the Fontan conduit were significantly different from 0.9 (i.e. uniform mixing), p<0.001 and p=0.012, respectively. The mixing of HV and IVC blood flows within the caudal and cranial part of the Fontan conduit for a typical extracardiac conduit Fontan patient is shown in Figure 1 and Video 1. The time-resolved mixing between HV and IVC flow in the four subsections at two different levels of the Fontan conduit is shown for a typical extracardiac Fontan patient (Figure 1D-E).

Table 1. Patient characteristics

Male/Female	9/6
BSA, m^2	1.6 (0.2)
Age at MRI, years	18.2 (5.6)
Fontan type (ECC/LT)	14/1
Conduit size (16/18/20 millimeter)	9/4/1
$Q_{IVC,}$ L/min	3.0 (0.7)
$Q_{HV,}$ L/min	1.5 (0.6)
Contribution of Q_{HV} to $Q_{conduit}$ (%)	32.7 (9.3)

Values are reported as mean (standard deviation). BSA; body surface area (Haycock), MRI; magnetic resonance imaging, ECC; extracardiac conduit, LT; lateral tunnel, Q; flowrate, IVC; inferior vena cava, HV; hepatic veins. L/min; liter per minute

When comparing $M_{average}$ at the four subsections in the caudal cross-section, $M_{average}$ at the right-posterior subsection was lowest, significantly lower compared to the right-anterior subsection (0.47±0.34 vs 0.76±0.20, respectively, p=0.03). No significant differences between other caudal subsections (left-posterior 0.68±0.29, left-anterior 0.65±0.24) were observed. $M_{average}$ was significantly different from 0.9 (i.e. uniform mixing) for all caudal subsections (all p-values <0.025). At the cranial level, no significant differences in $M_{average}$ were found between the four subsections: right-anterior (0.85±0.13), left-anterior (0.80±0.18), right-posterior (0.75±0.23) or left-posterior (0.73±0.19). $M_{average}$ was significantly different from 0.9 in the right and left posterior subsections (p=0.02 and P=0.004, respectively), indicating non-uniform mixing in these segments, but not in the right and left anterior subsections (p=0.2 and p=0.06, respectively).

HFD analysis

The result of the HFD analysis and comparison between the three methods are presented in Table 2 and Figure 3. No significant differences were found between $HFD_{caudal\ conduit}$ and $HFD_{cranial\ conduit}$ (p=0.80). However, when comparing the direct HFD_{HV} method with the conventional methods, significant differences were observed: HFD_{HV} (51.0±20.6%) versus $HFD_{caudal\ conduit}$ (p=0.033) as well as HFD_{HV} versus $HFD_{cranial\ conduit}$ (p=0.044). Although statistically significant, differences between the conventional and direct HFD quantification methods were relatively small, with differences <5% in 8/15 and 11/15 using the $HFD_{caudal\ conduit}$ and $HFD_{cranial\ conduit}$ methods, respectively. However, in individual subjects differences as high as 8.2-14.9% were observed in 4/15 patients.

No significant correlation was found for the absolute difference in HFD between the direct and both conventional methods and $M_{average}$ at the caudal or cranial conduit, respectively (r=0.32, p=0.27 and r=-0.06, p=0.82, respectively). The 4 patients with highest absolute differences between methods did not have a significantly different HV to IVC flow ratio (mean ratio 0.50 vs 0.54, p=0.41), pulsatility (Q_{max}-Q_{min}/Q_{mean}, where Q

is the flowrate) of the IVC (mean 0.40 vs 0.41, P=0.66) and conduit (mean 0.66 vs 0.53, p=0.41) or HV to conduit percentage (mean 32% vs 35%, p=0.75) compared to the 11 patients with smallest differences.

Table 2. Comparisons between HFD quantification methods

	Paired t-test	Bland-Altman		Intraclass Correlation	Mean absolute difference
Comparisons	P value	Mean difference	LoA	ICC	(±1.96 SEM)
HFD_{HV} vs $HFD_{caudal\ tunnel}$	**0.033**	2.9	-6.3–12.0	0.97	4.6(3.1-6.0)
HFD_{HV} vs $HFD_{cranial\ tunnel}$	**0.044**	3.1	-7.4–13.6	0.96	4.4(2.2-6.5)
$HFD_{caudal\ tunnel}$ vs $HFD_{cranial\ tunnel}$	0.80	0.2	-6.0–6.4	0.99	2.4(1.3-3.4)

HFD; hepatic flow distribution. SEM; standard error of the mean, LoA; limits of agreement, defined as the mean difference ±1.96 standard deviations.

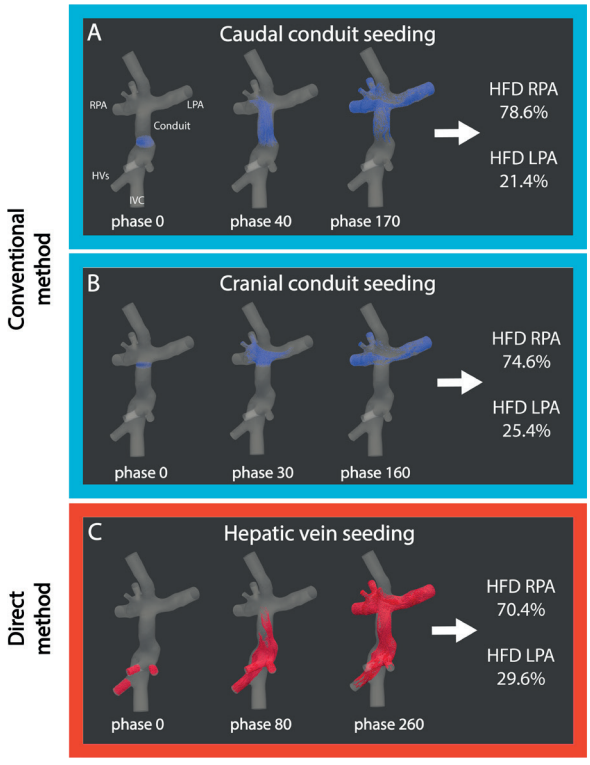

Figure 2. The three HFD quantification approaches are shown for a typical Fontan patient. Particles were uniformly seeded from the caudal or cranial conduit (conventional method) or directly from the hepatic veins (direct method). The starting position and the trajectory of these particles over time are shown for two cardiac phases. The percentage of particles arriving at each pulmonary artery were recorded representing the HFD.

IVC; inferior vena cava, HVs; hepatic veins, LPA/RPA; left/right pulmonary artery, HFD; hepatic flow distribution.

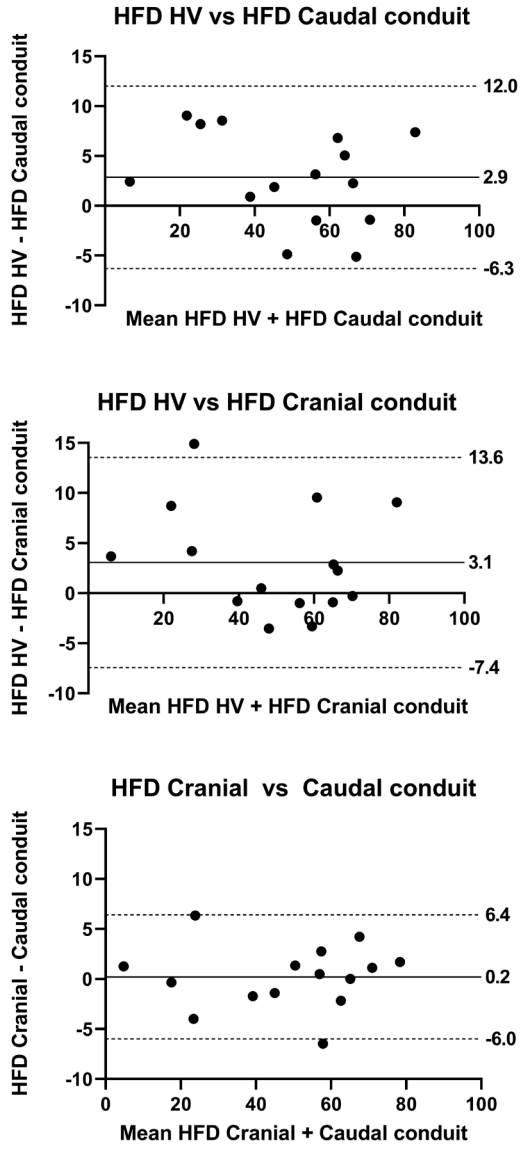

Figure 3. Bland-Altman plots comparing HFD measurements between the three different approaches. The mean difference + limits of agreement (±1.96 times the standard deviation) are shown in the plot.

Comment

This study incorporates the hepatic veins into patient-specific CFD models of the TCPC in Fontan patients, in order to assess mixing of HV and IVC flow and to allow for HFD quantification by tracking particles directly from the HVs. Main findings show that hepatic venous flow is not uniformly distributed within the Fontan conduit. This lack of uniform distribution was most evidently present at the caudal part of the Fontan conduit (just distal of the entry of the HVs into the IVC) with significantly better mixing of HV and IVC flows at the cranial part of the conduit. Tracking particles from the caudal or cranial part of the Fontan conduit did not result in significant different HFD despite these different mixing characteristics. However, tracking particles directly from the HVs (HFD_{HV}) was significantly different from both conventional HFD quantification methods (i.e. tracking Fontan conduit flow), although on a cohort-level differences were small. On an individual basis, however, differences of 8.2-14.9% in HFD were observed which may be of clinical importance.

HFD quantification is an important metric in the evaluation of the TCPC in Fontan patients, since there is compelling evidence for a strong association between a lack of HV flow towards the lung and the formation of pulmonary arteriovenous malformations[2]. Therefore, identification of an unbalanced HFD may indicate the need for intervention aiming to restore a more balanced HFD. Furthermore, when an intervention of the TCPC is considered, virtual surgery platforms offer the possibility to evaluate multiple different TCPC geometries[1, 12, 20]. Subsequently, the optimal geometry with minimal power loss while ensuring a balanced HFD can be selected[6, 21, 22]. The accuracy of the HFD quantification method itself, however, has not been studied.

The conventional approach for HFD quantification relies on the assumption that hepatic venous flow, theoretically taking up to approximately 38% of total Fontan conduit flow[23], is uniformly distributed within the Fontan conduit and thus can be used interchangeably. This study showed that this assumption is not valid, most evident at the level just above the entry of the hepatic veins into the IVC. The HV flow and IVC flow demonstrate two different flow streams with only moderate mixing during the cardiac cycle. This can be explained by the fact that blood flow in the Fontan conduit is in general laminar with only minimal pulsatility along the cardiac cycle preventing thorough mixing of both flows. The right-posterior part of the caudal Fontan conduit showed lowest mixing of HV with IVC flow as the anatomy of the IVC and HVs likely resulted in less HV flow particularly in this segment. At the cranial side of the Fontan conduit, as both flows had more time to interact, significantly improved mixing was present but still non-uniform mixing was observed.

Therefore, using Fontan conduit flow as a surrogate of HV flow will introduce inaccuracies in HFD quantification. This study shows that on a cohort-level the anticipated inaccuracy is small and of minimal clinical relevance. Therefore, the fact that HV flow is not uniformly distributed in the Fontan conduit does in general not seem to make a significant difference in HFD quantification, with 95% of mean absolute differences expected to be <6.1-6.5% making previous obtained results on a cohort-level valid[3, 20]. Furthermore, results also indicated that when the conventional HFD quantification is used, starting position of the particles (from the caudal or cranial conduit) did not result in significantly different HFD, despite the difference in mixing characteristics.

Although differences were small on a cohort-level, it should be noted that on an individual basis, differences of 8.2-14.9% were observed in 4/15 patients which may have impact on patient-specific clinical decision making. For example, in the patient with the largest difference, HFD was only 20.7% by tracking cranial conduit flow, while HFD was 35.6% when directly tracking HV flow. Although the minimal amount of HFD to prevent the formation of pulmonary arteriovenous malformations is not clear, a minimum HFD of 30% towards a lung has been suggested to be clinical acceptable[13, 22, 24]. For this patient, therefore, the conventional method would imply insufficient HFD, while direct HV flow tracking shows sufficient HV flow towards the LPA. Since virtual surgery platforms are used for pre-interventional planning on an individual basis, incorporating hepatic veins into the patient-specific CFD models might have impact for at least some patients. As for the majority of patients the differences were small, it would be interesting to investigate if certain flow or geometric characteristics, which can show a wide variability at the level where the IVC and HVs join[25], can help identify the patients with the largest inaccuracies that would benefit most from direct HFD quantification. Because of the limited number of patients this question could not be answered in this study. Larger numbers are needed in future studies to identify anatomical and/or flow characteristics to identify patients with important differences in direct and indirect HFD quantification.

Limitations

Although this study reveals important, novel insights into the flow dynamics of HV and IVC flow within the Fontan conduit and its influence on HFD quantification, some limitations are present. Although the sample size is relatively small, significant differences between methods could be detected with considerable differences on a patient-specific level. Furthermore, no direct hepatic venous flow measurements were acquired which were considered clinically unfeasible, by requiring multiple extra survey scans to plan 3-6 extra 2D flow measurements in relatively small vessels. We assumed total hepatic venous flow to be distributed over the respective HVs by the ratio of their respective cross-sectional areas. Future studies should aim on obtaining direct measurements of HV flow in Fontan patients, for example using 4D flow MRI,

to further increase the accuracy of HV flow modelling in these patients. In addition, ECG-gated, free-breathing 2D PC-MRI was used as boundary conditions, which does not take respiration effects on hepatic flow into account. Previous studies have shown that hepatic venous flow can increase up to 3-fold during inspiration while having minimal effect on IVC flow[23], which may influence HV streaming patterns and subsequent HFD quantification. Also, predominantly extracardiac conduit Fontan patients were included in this study, and possible different flow characteristics in lateral tunnel patients may provide different results. Furthermore, a relatively coarse assessment of mixing was performed by dividing the cross-section of the Fontan conduit in only 4 parts. Therefore, mixing on a smaller scale was not taken into account.

Conclusion

In conclusion, hepatic venous flow is non-uniformly distributed within the Fontan conduit. Evident separate HV and IVC flow streaming patterns were present, most clearly just above entry of the HVs into the IVC. On a cohort-level, significant but small differences in HFD were observed when comparing direct (tracking hepatic venous flow) and conventional methods (tracking Fontan conduit flow). However, individual differences of 8.2-14.9% in HFD were observed in a subset of patients which may be of clinical importance by affecting accurate identification of patients with unbalanced HFD or by affecting optimal TCPC geometry selection when using virtual surgery platforms.

References

1. Rijnberg FM, Hazekamp MG, Wentzel JJ, de Koning PJH, Westenberg JJM, Jongbloed MRM, Blom NA, Roest AAW. Energetics of Blood Flow in Cardiovascular Disease: Concept and Clinical Implications of Adverse Energetics in Patients With a Fontan Circulation. Circulation 2018;137(22):2393-2407.
2. Kavarana MN, Jones JA, Stroud RE, Bradley SM, Ikonomidis JS, Mukherjee R. Pulmonary arteriovenous malformations after the superior cavopulmonary shunt: mechanisms and clinical implications. Expert Rev Cardiovasc Ther 2014;12(6):703-13.
3. Haggerty CM, Restrepo M, Tang E, de Zelicourt DA, Sundareswaran KS, Mirabella L, Bethel J, Whitehead KK, Fogel MA, Yoganathan AP. Fontan hemodynamics from 100 patient-specific cardiac magnetic resonance studies: a computational fluid dynamics analysis. J Thorac Cardiovasc Surg 2014;148(4):1481-9.
4. Yang W, Chan FP, Reddy VM, Marsden AL, Feinstein JA. Flow simulations and validation for the first cohort of patients undergoing the Y-graft Fontan procedure. J Thorac Cardiovasc Surg 2015;149(1):247-55.
5. de Zelicourt DA, Marsden A, Fogel MA, Yoganathan AP. Imaging and patient-specific simulations for the Fontan surgery: current methodologies and clinical applications. Prog Pediatr Cardiol 2010;30(1-2):31-44.
6. Trusty PM, Slesnick TC, Wei ZA, Rossignac J, Kanter KR, Fogel MA, Yoganathan AP. Fontan Surgical Planning: Previous Accomplishments, Current Challenges, and Future Directions. J Cardiovasc Transl Res 2018;11(2):133-144.
7. Bachler P, Valverde I, Pinochet N, Nordmeyer S, Kuehne T, Crelier G, Tejos C, Irarrazaval P, Beerbaum P, Uribe S. Caval blood flow distribution in patients with Fontan circulation: quantification by using particle traces from 4D flow MR imaging. Radiology 2013;267(1):67-75.
8. Jarvis K, Schnell S, Barker AJ, Garcia J, Lorenz R, Rose M, Chowdhary V, Carr J, Robinson JD, Rigsby CK, Markl M. Evaluation of blood flow distribution asymmetry and vascular geometry in patients with Fontan circulation using 4-D flow MRI. Pediatr Radiol 2016;46(11):1507-19.
9. Bastkowski R, Bindermann R, Brockmeier K, Weiss K, Maintz D, Giese D. Respiration Dependency of Caval Blood Flow in Patients with Fontan Circulation: Quantification Using 5D Flow MRI. Radiology: Cardiothoracic Imaging 2019;1(4):e190005.
10. Rutkowski D, Medero R, Ruesink T, Roldan-Alzate A. Modeling Physiological Flow Variation in Fontan Models with 4d Flow Mri, Particle Image Velocimetry, and Arterial Spin Labeling. J Biomech Eng 2019.
11. Rutkowski DR, Barton G, Francois CJ, Bartlett HL, Anagnostopoulos PV, Roldan-Alzate A. Analysis of cavopulmonary and cardiac flow characteristics in fontan Patients: Comparison with healthy volunteers. J Magn Reson Imaging 2019;49(6):1786-1799.
12. Dasi LP, Whitehead K, Pekkan K, de Zelicourt D, Sundareswaran K, Kanter K, Fogel MA, Yoganathan AP. Pulmonary hepatic flow distribution in total cavopulmonary connections: extracardiac versus intracardiac. J Thorac Cardiovasc Surg 2011;141(1):207-14.
13. Trusty PM, Restrepo M, Kanter KR, Yoganathan AP, Fogel MA, Slesnick TC. A pulsatile hemodynamic evaluation of the commercially available bifurcated Y-graft Fontan modification and comparison with the lateral tunnel and extracardiac conduits. J Thorac Cardiovasc Surg 2016;151(6):1529-36.
14. Yang W, Feinstein JA, Shadden SC, Vignon-Clementel IE, Marsden AL. Optimization of a Y-graft design for improved hepatic flow distribution in the fontan circulation. J Biomech Eng 2013;135(1):011002.

15. Yushkevich PA, Piven J, Hazlett HC, Smith RG, Ho S, Gee JC, Gerig G. User-guided 3D active contour segmentation of anatomical structures: significantly improved efficiency and reliability. Neuroimage 2006;31(3):1116-28.
16. Antiga L, Piccinelli M, Botti L, Ene-Iordache B, Remuzzi A, Steinman DA. An image-based modeling framework for patient-specific computational hemodynamics. Med Biol Eng Comput 2008;46(11):1097-112.
17. Trusty PM, Wei Z, Sales M, Kanter KR, Fogel MA, Yoganathan AP, Slesnick TC. Y-graft modification to the Fontan procedure: Increasingly balanced flow over time. J Thorac Cardiovasc Surg 2019.
18. Wei Z, Singh-Gryzbon S, Trusty PM, Huddleston C, Zhang Y, Fogel MA, Veneziani A, Yoganathan AP. Non-Newtonian Effects on Patient-Specific Modeling of Fontan Hemodynamics. Ann Biomed Eng 2020.
19. Yang W, Vignon-Clementel IE, Troianowski G, Reddy VM, Feinstein JA, Marsden AL. Hepatic blood flow distribution and performance in conventional and novel Y-graft Fontan geometries: a case series computational fluid dynamics study. J Thorac Cardiovasc Surg 2012;143(5):1086-97.
20. Tang E, Restrepo M, Haggerty CM, Mirabella L, Bethel J, Whitehead KK, Fogel MA, Yoganathan AP. Geometric characterization of patient-specific total cavopulmonary connections and its relationship to hemodynamics. JACC Cardiovasc Imaging 2014;7(3):215-24.
21. Slesnick TC, Yoganathan AP. Computational modeling of Fontan physiology: at the crossroads of pediatric cardiology and biomedical engineering. Int J Cardiovasc Imaging 2014;30(6):1073-84.
22. Sundareswaran KS, de Zelicourt D, Sharma S, Kanter KR, Spray TL, Rossignac J, Sotiropoulos F, Fogel MA, Yoganathan AP. Correction of pulmonary arteriovenous malformation using image-based surgical planning. JACC Cardiovasc Imaging 2009;2(8):1024-30.
23. Hsia TY, Khambadkone S, Redington AN, Migliavacca F, Deanfield JE, de Leval MR. Effects of respiration and gravity on infradiaphragmatic venous flow in normal and Fontan patients. Circulation 2000;102(19 Suppl 3):III148-53.
24. Wei ZA, Trusty PM, Tree M, Haggerty CM, Tang E, Fogel M, Yoganathan AP. Can time-averaged flow boundary conditions be used to meet the clinical timeline for Fontan surgical planning? J Biomech 2017;50:172-179.
25. Rijnberg FM, Elbaz MSM, Westenberg JJM, Kamphuis VP, Helbing WA, Kroft LJ, Blom NA, Hazekamp MG, Roest AAW. Four-dimensional flow magnetic resonance imaging-derived blood flow energetics of the inferior vena cava-to-extracardiac conduit junction in Fontan patients. Eur J Cardiothorac Surg 2019;55(6):1202-1210.

Supplementary materials

Supplemental table 1. MRI details of TCPC anatomic and velocity acquisitions

MRI details	2D transversal and sagittal stacks	2D PC-MRI
Slice thickness (mm)	5, 2.5 overlap	5
Acquired in-plane spatial resolution (mm)	1.76x1.74	1.5 x 1.5
Reconstructed in-plane spatial resolution (mm)	0.9 x 0.9 mm	0.6 x 0.6
Acquired temporal resolution (ms)	-	41.0 (12.2)
Nr of phases per cardiac cycle	-	25-30
ECG-gating	-	retrospective
Respiratory compensation	navigator	-
Acceleration methods	SENSE factor 1.5	Segmentation factor 1-2, SENSE factor 1.4

All MRI examinations were performed on a 3T Philips MRI scanner (Ingenia, Philips Healthcare, Best, the Netherlands).

mm; millimetre, ECG; electrocardiogram, PC-MRI; phase contrast magnetic resonance imaging

Supplementary material 1

3D reconstruction of the TCPC

In order to perform CFD, a 3D reconstruction of the TCPC is required. As a first step, automatic, rigid registration was performed of the transversal and sagittal anatomic MRI stacks to correct for possible spatial misalignment between both acquisitions (ITK-SNAP). Images were interpolated (linear) and the TCPC was subsequently segmented on both views using a semi-automatic, active contour method with manual adjustment. The segmented TCPC covered the area between the subhepatic IVC, hepatic veins, SVC, RPA and LPA. Segmental branches were excluded, except for the right upper lobe branches. A 3D TCPC model was reconstructed and smoothed using a non-shrinking Taubin filter (500 iterations, Passband 0.05), and centerlines were derived for each vessel (VMTK).

CFD simulations

All in- and outlets of the 3D TCPC model were clipped perpendicular to the centerlines and vessel extensions were added. The hepatic veins were clipped close to the connection with the IVC and most often included a right, middle and left hepatic vein. In case of hepatic vein subbranching close to the connection with the IVC, the hepatic veins were clipped more away from the IVC into separate subbranches. In this way, the diameter

or inflow angle of the hepatic vein into the IVC was consolidated. After performance of a mesh-independence study, the TCPC geometries were meshed with 30 polyhedral elements across the average vessel diameter (range 0.4-0.5mm elements) in order to achieve mesh-independent results, including a four prism layer at the vessel walls (ANSYS ICEM CFD v17.1, ANSYS, Inc., Canonsburg, PA). The total number of elements ranged from 1.5 to 2.7 million. All CFD simulations were performed using commercially available Fluent software (v17.1, ANSYS, Inc., Canonsburg, PA).

Time-resolved flowrates were prescribed with a parabolic velocity profile at the inlets. Total hepatic venous flow was divided over the multiple hepatic veins on the basis of the ratio of their respective cross-sectional areas. Outlet boundary conditions were imposed based on the ratio of the pulmonary flow distribution (total RPA/total LPA flow divided by the total PA flow). The right pulmonary flow distribution was divided over the RPA branches based on their respective cross-sectional areas.[1] In case RPA flow was measured distal to the branch towards the right upper lobe, firstly flow towards the right upper lobe was calculated based on the ratio of the cross sectional area of the distal RPA and right upper lobe branch. In these cases, total RPA flow was determined by the sum of the distal RPA flow and calculated flow towards the right upper lobe branch. A rigid vessel wall was assumed and a no-slip condition prescribed. Blood flow was assumed to be laminar. The blood was considered as an incompressible fluid with a density of 1060 kg/m3. A Carreau model was used to account for the non-Newtonian blood properties in the TCPC. The convergence criteria was set to 10^{-4}. Unsteady CFD simulations were performed for 7 cardiac cycles, simulating 1000 time-steps per cycle. The results of the last 4 cycles were used for the hepatic blood flow mixing and HFD analysis.

Reference

[1] Haggerty CM, Restrepo M, Tang E, de Zelicourt DA, Sundareswaran KS, Mirabella L, Bethel J, Whitehead KK, Fogel MA, Yoganathan AP. Fontan hemodynamics from 100 patient-specific cardiac magnetic resonance studies: a computational fluid dynamics analysis. J Thorac Cardiovasc Surg 2014;148(4):1481-9.

Supplementary material 2

Quantification of mixing between IVC and Hepatic blood flow

A method to quantify mixing of hepatic and IVC blood flow within the Fontan conduit was developed based on the spatial distribution of both flows using particle tracing

(Paraview.org). A total of 7500 particles were released from the hepatic veins for each time-step during 5 cardiac cycles. The number of particles per hepatic vein was based on the ratio of their respective cross-sectional areas. The amount of particles released from the subhepatic IVC was based on the average flow ratio between the IVC and hepatic veins; 7500 x $\frac{Q_{IVC}}{Q_{HV}}$.

Pathlines, representing the trajectory each particle follows over time, were generated and transections with these pathlines were made at two cross-sections with the Fontan conduit, perpendicular to its centerline: the caudal part of the Fontan conduit, just above the connection between the Fontan conduit with the IVC/HVs, and at the cranial part of the Fontan conduit, just below the connection with the PA (Figure 1A-C, Video 1). IVC and HV pathline transections at each cross-section of the Fontan conduit were recorded for each time-step in the 5th cardiac cycle. The ideal mixing of HV and IVC blood flow was determined by the ratio between the number of IVC and HV pathlines for each time-step at both positions in the Fontan conduit (ideal mixing ratio HV: R_{mixing_HV} and ideal mixing ratio IVC: R_{mixing_IVC}):

(1) Ideal mixing ratio HV, R_{mixing_HV}: $\frac{P_{HV}}{P_{total}}$, ϵ [0,1]

(2) Ideal mixing ratio IVC, R_{mixing_IVC}: $\frac{P_{IVC}}{P_{total}}$, ϵ [0,1]

where P_{HV}= number of HV pathlines in the entire cross-section, P_{IVC}= number of IVC pathlines in the entire cross-section, $P_{total} = P_{HV}+P_{IVC;}$ $R_{mixing_HV} = 1 - R_{mixing_IVC}$.

Subsequently, both caudal and cranial Fontan conduit cross-sections were manually subdivided in a right-left and anterior-posterior direction, resulting in four sections: left-anterior, left-posterior, right-anterior and right-posterior (Figure 1B-C). The mixing of HV and IVC blood flow within each of these four sections was quantified as follows:

(3) Measured mixing ratio HV in each section, $R^*_{mixing_HV}$: $\frac{P^*_{HV}}{P^*_{total}}$, ϵ [0,1]

(4) Measured mixing ratio IVC in each section, $R^*_{mixing_IVC}$: $\frac{P^*_{IVC}}{P^*_{total}}$, ϵ [0,1]

where, P^*_{HV}= number of HV pathlines in the section, P^*_{IVC}= number of IVC pathlines in the section, $P^*_{total} = P^*_{HV}+P^*_{IVC}$, $R^*_{mixing_HV} = 1 - R^*_{mixing_IVC}$

The relative mixing ratio in each section, defined as the ratio between the ideal (based on the entire cross-section) and measured mixing ratio (within each section), was determined as follows:

(5) Relative mixing ratio HV, m_{HV}: m_{HV}: $\frac{R^*mixing_HV}{Rmixing_HV}$

(6) Relative mixing ratio IVC, m_{IVC}: m_{IVC}: $\frac{R^*mixing_IVC}{Rmixing_IVC}$

Finally, HV and IVC blood flow mixing (M) in each section was defined as the minimal value of relative mixing ratios (Supplemental Figure 1):

(7) Mixing (M) in each section = $\min(m_{HV}, m_{IVC}) \in [0,1]$

A mixing (M) of 0 indicates no mixing (only HV or IVC pathlines present in the section) and 1 indicates perfect mixing (the exact same ratio of HV and IVC pathlines in the section as in the entire cross-section (ideal mixing ratio)). A mixing value between 0 and 1, e.g. 0.4, can be interpreted as 60% less pathlines, either HV or IVC, are present in the section as expected based on the ideal mixing ratio. Therefore, this mixing parameter can quantify and visualize mixing characteristics within each of the four sections in the different levels of the Fontan conduit for each time-step in the cardiac cycle (Figure 1D-E). However, this mixing parameter cannot distinguish whether poor mixing is caused by an underrepresentation of HV or IVC blood flow in a section, which might change during the cardiac cycle (i.e. poor mixing in a section can be due to underrepresentation of HV flow in one phase but due to underrepresentation of IVC flow in another phase, leading to improved mixing in that section when averaged over time). Therefore, cardiac-cycle averaged mixing ($M_{average}$) was determined for each section by using the average number of HV and IVC pathlines present during the cardiac cycle (i.e. taking the sum of IVC and HV pathlines in each section for each phase in the cardiac cycle divided by the total number of phases). $M_{average}$ per section was weighted by the area of the section (area section/total area cross-section) and summed to obtain $M_{average}$ for the entire cross-section.

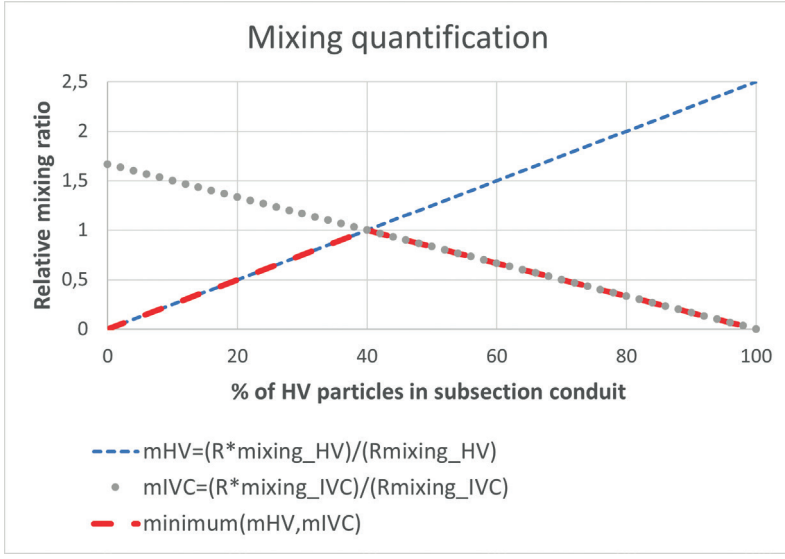

Supplemental Figure 1. The graph shows an example of the calculation of the mixing between hepatic venous blood (HV) and inferior vena caval blood (IVC). In this example, the ideal mixing ratio (Rmixing_HV) for the HV was 0.4 and the ideal mixing ratio for the IVC (Rmixing_IVC) was 0.6. As noted from the graph, when the measured mixing ratio for the HV in a section of the conduit (R*mixing_HV) is also 0.4 (the ideal case), than the relative mixing ratio mHV (i.e. the ratio between the measured and ideal mixing ratio) is 1. When R*mixing_HV is larger than 0.4 (i.e. more HV blood is present in the section than would be expected from the ratio of HV and IVC blood within the entire cross-section, which is suboptimal mixing), mHV will be larger than 1 but mIVC will be smaller than 1 (because less IVC blood will be present in that section than expected). Therefore, to determine the mixing of HV and IVC flow on a scale between 0 and 1, the minimum of mHV and mIVC is taken. As a result, a mixing of 0.7 indicates that 30% less HV or IVC pathlines were present in a certain subsection compared to what would be expected from the ratio of IVC and HV pathlines in the entire cross-section.